

X-Point Collapse and Saturation in the Nonlinear Tearing Mode Reconnection

N. F. Loureiro,¹ S. C. Cowley,^{1,2} W. D. Dorland,³ M. G. Haines,¹ and A. A. Schekochihin⁴

¹Plasma Physics Group, Blackett Laboratory, Imperial College, Prince Consort Road, London SW7 2BW, United Kingdom

²Department of Physics and Astronomy, UCLA, Los Angeles, California 90095-1547, USA

³Department of Physics, University of Maryland, College Park, Maryland 20742-3511, USA

⁴DAMTP, University of Cambridge, Cambridge CB3 0WA, United Kingdom

(Received 31 July 2005; published 29 November 2005)

We study the nonlinear evolution of the resistive tearing mode in slab geometry in two dimensions. We show that, in the strongly driven regime (large Δ'), a collapse of the X point occurs once the island width exceeds a certain critical value $\sim 1/\Delta'$. A current sheet is formed and the reconnection is exponential in time with a growth rate $\propto \eta^{1/2}$, where η is the resistivity. If the aspect ratio of the current sheet is sufficiently large, the sheet can itself become tearing-mode unstable, giving rise to secondary islands, which then coalesce with the original island. The saturated state depends on the value of Δ' . For small Δ' , the saturation amplitude is $\propto \Delta'$ and quantitatively agrees with the theoretical prediction. If Δ' is large enough for the X-point collapse to have occurred, the saturation amplitude increases noticeably and becomes independent of Δ' .

DOI: 10.1103/PhysRevLett.95.235003

PACS numbers: 52.35.Vd, 52.35.Py, 52.65.Kj

Magnetic reconnection is the breaking and rejoining of magnetic field lines in a plasma. Solar flares are believed to be a manifestation of this phenomenon [1]. Other classical examples are reconnection between the solar and Earth's magnetic field in the magnetopause and the magnetotail [2] and the sawtooth instability in tokamaks [3]. In some cases, most notably the sawtooth, reconnection takes place in a plane perpendicular to a strong magnetic field, in which case it occurs via the tearing-mode instability. Linear theory [4] shows that an MHD equilibrium is tearing-mode unstable if the instability parameter $\Delta' > 0$. Analytical and numerical studies of the tearing mode have been mostly restricted to low values of Δ' . However, it has been shown that kinetic effects can change the instability threshold to $\Delta' > \Delta'_{\text{crit}} \gg 1$ [5,6], and there is, indeed, experimental evidence for $\Delta' \gg 1$ in the sawtooth (see, e.g., [7] and references therein). The evolution of large- Δ' (i.e., strongly driven) tearing modes, even in the simplest physical models, remains poorly understood. To address this problem, we investigate the evolution of the tearing mode in the broadest ranges of Δ' and the resistivity η achieved to date. We find that, for sufficiently large Δ' and sufficiently small η , the tearing mode goes through five stages (Fig. 1): (I) linear instability [4], (II) algebraic growth (Rutherford [8] stage), (III) X-point collapse followed by current-sheet reconnection (Sweet-Parker [9,10] stage), (IV) tearing instability of the current sheet resulting in generation of secondary islands, and (V) saturation. The traditional theory of the tearing mode, valid for small Δ' , comprises just stages I, II, and V. A quantitative characterization of stages III–V is the subject of this Letter.

We solve the reduced MHD equations [11],

$$\partial_t \omega + \mathbf{v}_\perp \cdot \nabla \omega = \mathbf{B}_\perp \cdot \nabla j_\parallel, \quad (1)$$

$$\partial_t \psi + \mathbf{v}_\perp \cdot \nabla \psi = \eta \nabla^2 \psi, \quad (2)$$

in a two-dimensional periodic box $L_x \times L_y$ using a pseudospectral code at resolutions up to 3072×4096 . The total magnetic field is $\mathbf{B} = B_z \mathbf{e}_z + \mathbf{B}_\perp$, the in-plane magnetic field is $\mathbf{B}_\perp = \mathbf{e}_z \times \nabla \psi$, the in-plane velocity is $\mathbf{v}_\perp = \mathbf{e}_z \times \nabla \phi$, and $\omega = \mathbf{e}_z \cdot (\nabla \times \mathbf{v}_\perp) = \nabla^2 \phi$, $j_\parallel = \mathbf{e}_z \cdot (\nabla \times \mathbf{B}) = \nabla^2 \psi$. We impose the equilibrium configuration $\psi^{(0)} = \psi_0 / \cosh^2(x)$ and $\phi^{(0)} = 0$. By setting $\psi_0 = 3\sqrt{3}/4$, we scale the units of field strength in such a way that the maximum value of $B_y^{(0)} = d\psi^{(0)}/dx$ is $B_{y,\text{max}}^{(0)} = 1$. All lengths are scaled so that $L_x = 2\pi$. Time is, therefore, scaled by the in-plane Alfvén time $L_x/2\pi B_{y,\text{max}}^{(0)}$. To the equilibrium, we add an initial perturbation $\psi^{(1)} = \psi_1(x) \times \cos(ky)$, where $k = L_x/L_y$. Given a perturbation in this form, the island width W and the reconnected flux $\Psi(t) = -\psi(t, 0, 0) + \psi_0$ are related by

$$W = 4\sqrt{\Psi(t)/\psi_0''(0)}. \quad (3)$$

For our equilibrium, the instability parameter is [12]

$$\Delta' = \frac{\psi_1'(0) - \psi_1'(-0)}{\psi_1(0)} = \frac{2(5 - k^2)(3 + k^2)}{k^2\sqrt{4 + k^2}}. \quad (4)$$

The equilibrium is tearing unstable if $\Delta' > 0 \Leftrightarrow k < \sqrt{5}$. Δ' is varied by changing k , i.e., L_y .

We now describe the evolution of the tearing-mode stage by stage. During stages I–II, reconnection occurs via an X-point configuration. In stage I, it is a linear instability with the island width W growing exponentially in time [4]. Once W exceeds the resistive scale, this stage gives way to the Rutherford [8] stage (stage II), during which the growth is algebraic in time: $dW/dt \sim \eta\Delta'$. Omitting further discussion of these stages, which have been studied before [13], we proceed to stage III.

Stage III: X-point collapse and Sweet-Parker (SP) reconnection.—Waelbroeck [14] predicted that when the island width $W > W_c \approx 25/\Delta'$, the X point should collapse

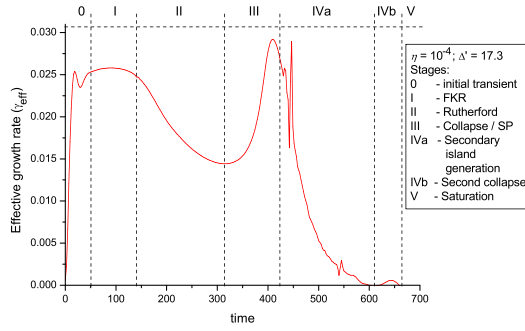


FIG. 1 (color online). Effective growth rate at the X point $\gamma_{\text{eff}} = d \ln \Psi / dt$ vs time for a strongly driven (large Δ') tearing mode. FKR stands for Furth-Killeen-Rosenbluth, after the authors of Ref. [4].

to a current sheet. Indeed, in simulations with large Δ' , the X-point configuration eventually collapses and a current sheet is formed (Fig. 2) accompanied by a dramatic speed up of the island growth (Fig. 1). A clear numerical demonstration of this was recently reported by Jemella *et al.* [15] (see also earlier results [16]). In our simulations, we have varied η and Δ' to verify Waelbroeck's transition criterion. We define W_c as the island width at which $d\gamma_{\text{eff}}/dt = 0$ after the Rutherford-like algebraic stage (e.g., at $t \approx 315$ in Fig. 1). In Fig. 3, we plot $\Delta'W_c$ vs η for two different values of Δ' . The dependence of $\Delta'W_c$ on η appears to be linear and extrapolates in the limit of $\eta \rightarrow 0$ to $\Delta'W_c \approx 8.2$ for both values of Δ' used. Thus, the transition criterion is

$$\Delta'W_c \approx 8.2 + f(\Delta')\eta, \quad (5)$$

where $f(\Delta')$ is undetermined but is seen in Fig. 3 to increase with Δ' . Equation (5) confirms Waelbroeck's scaling of W_c with Δ' , but not his numerical prefactor. The numerical determination of the scaling (5) is a new result.

Figure 4(a) shows that, in this stage, the reconnected flux (measured at $x = y = 0$) grows exponentially in time: $\ln(\Psi - \Psi_c) = \gamma_{\text{SP}}(t - t_c)$, where t_c is the time at which the collapse begins, $\Psi_c = \Psi(t_c)$, and γ_{SP} is the growth rate [17]. Varying Δ' , we have ascertained that γ_{SP} is independent of Δ' . Its dependence on η is plotted in Fig. 4(b). The scaling $\gamma_{\text{SP}} \propto \eta^{1/2}$ appears to hold.

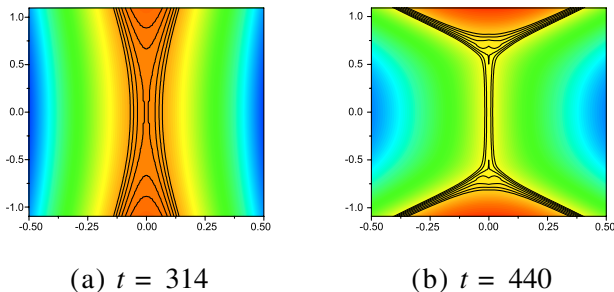


FIG. 2 (color online). Contours of ψ at the beginning and end of stage III in Fig. 1. The boundaries of these plots are *not* the boundaries of the computational box.

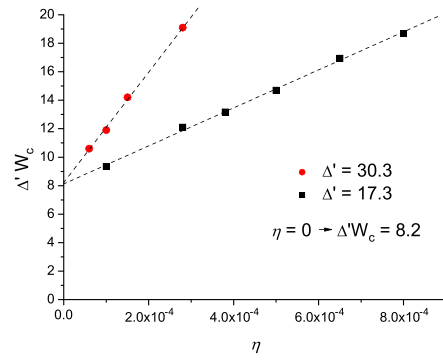


FIG. 3 (color online). The critical island width for collapse vs η at fixed $\Delta' = 17.3, 30.3$. Dashed lines are linear fits.

We think that what we observe is an exponential-in-time SP reconnection that proceeds qualitatively in the way described in [9,10] but with the outflow velocity v_{out} and the current-sheet length L_{CS} growing with time. Since the reconnected flux Ψ changes at the SP rate $\propto \eta^{1/2}$, we can assume that the evolution is quasistatic, so that the system passes through a sequence of ideal equilibria, in each of which L_{CS} and the configuration outside (but not inside) the current sheet are fully determined by the instantaneous value of Ψ . Let us assume that, in these equilibria, the vicinity of the current sheet is described by the Syrovatskii solution with a unidirectional current [18]. In this solution, the magnetic field immediately outside the sheet is $B_{\text{in}} = B_0(\Psi)L_{\text{CS}}(\Psi)/L_x$, where $\Psi = \Psi(t)$ is the reconnected flux and B_0 is the field away from the sheet. Then the reconnected flux grows according to (cf. [15,19,20])

$$d\Psi/dt \sim v_{\text{in}}B_{\text{in}} \sim \eta^{1/2}[B_0(\Psi)/L_x]^{3/2}L_{\text{CS}}(\Psi), \quad (6)$$

where we have used the SP expression for the inflow velocity, $v_{\text{in}} \sim (\eta v_{\text{out}}/L_{\text{CS}})^{1/2}$ and taken the outflow velocity to be Alfvénic, $v_{\text{out}} \sim B_{\text{in}}$. Equation (6) implies that the growth of Ψ must speed up compared to $\Psi \propto (\eta\Delta')^2$ in the Rutherford [8] stage (stage II). When Ψ is close to its value Ψ_c at the beginning of the collapse, we may approximate $B_0(\Psi) \sim B_0(\Psi_c) = \text{const}$. This implies $v_{\text{out}}/L_{\text{CS}} \sim B_{\text{in}}/L_{\text{CS}} \sim B_0/L_x = \text{const}$, a conclusion confirmed by Fig. 5(a). Since $L_{\text{CS}}(\Psi_c) = 0$, L_{CS} should be a growing function of $\Psi - \Psi_c$. Indeed, Eq. (6) is consistent with the

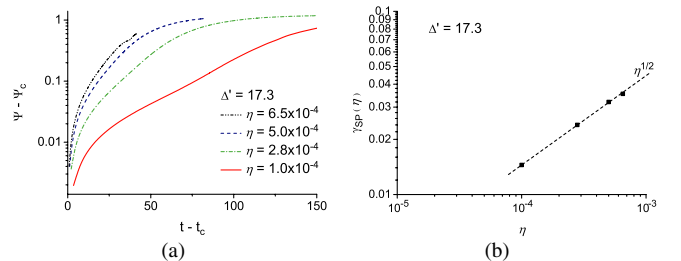


FIG. 4 (color online). (a) Growth of the reconnected flux Ψ during the SP stage for fixed $\Delta' = 17.3$ and various values of η . (b) Slopes of these lines vs η during the exponential growth.

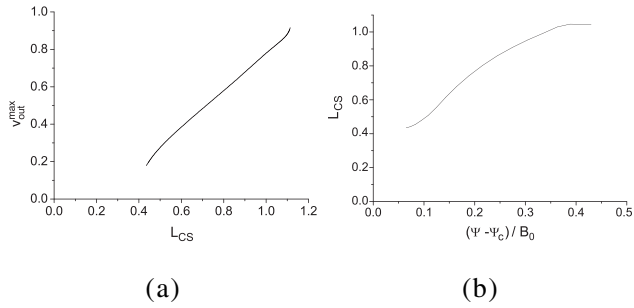


FIG. 5. The exponential stage ($370 < t < 450$) of the run of Fig. 1: (a) maximum outflow velocity v_{out} vs the current-sheet length L_{CS} ; (b) L_{CS} vs $(\Psi - \Psi_c)/B_0$, where B_0 is defined as the maximum value of B_y along the x axis. These curves do not extrapolate to the origin because the full-width-half-maximum definition used for L_{CS} correctly reflects the growth of the current-sheet length but not its true length (thus, it formally gives $L_{CS} > 0$ for the X -point reconnection).

numerically observed exponential SP reconnection if $L_{CS} \sim (\Psi - \Psi_c)/B_0$ [cf. Fig. 5(b)].

The elongation of the current sheet ceases when L_{CS} reaches a significant fraction of the box size. Reconnection can still proceed in a SP fashion, but the growth of the reconnected flux slows down (see Fig. 1). Indeed, in the right-hand side of Eq. (6), L_{CS} no longer increases with Ψ and $B_0(\Psi)$ starts to decrease as the initial reconnectable flux is used up. In Fig. 6, we show the current-sheet length L_{CS} and width δ_{CS} measured using a full-width-half-maximum estimate at the time when the maximum L_{CS} is reached. We see that, for fixed Δ' , L_{CS} is roughly independent of η , while $\delta_{CS} \sim \eta^{1/2}$, in agreement with the SP prediction. On the other hand, for fixed η , both L_{CS} and δ_{CS} grow with Δ' (cf. [21]). Note that for $\Delta' \gg 1$ we have $\Delta' \approx 15/k^2 \propto L_y^2$ [see Eq. (4)]. Since L_{CS} cannot exceed the box length L_y , it must, at large Δ' , grow no faster than $\sqrt{\Delta'}$.

Stage IV: Secondary-island generation.—When the aspect ratio of the current sheet $A = L_{CS}/\delta_{CS} \gtrsim 50$, the sheet becomes unstable and generates secondary islands. We expect that this critical value is independent of either Δ' or η , but due to resolution constraints, we do not yet have a numerical confirmation of this conjecture.

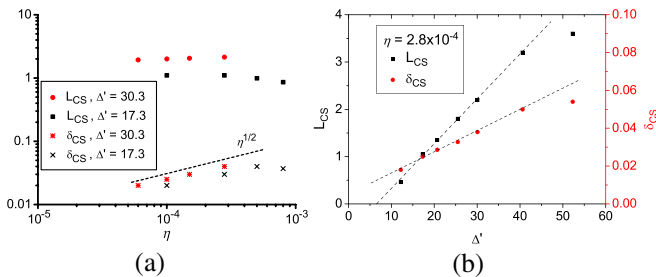


FIG. 6 (color online). The current-sheet length L_{CS} and width δ_{CS} (a) vs η and (b) vs Δ' .

Instability of the current sheets is a (numerically) known phenomenon [13,22,23], but no mathematical theory of it exists. In Fig. 7, we give the most detailed view of the instability affordable at current resolutions. As predicted in [24], a secondary island first appears as a long-wavelength linear perturbation to the current sheet, with two X points forming at the ends of the sheet [Fig. 7(b)]. This suggests that the theory of [24], while not mathematically rigorous, nevertheless captures the essential physics. Reconnection proceeds in a manner analogous to stages I–III discussed above: as the secondary island grows, the two secondary X points collapse, giving rise to two current sheets, while the island is circularized [Fig. 7(c)]. The primary and the secondary islands exert attracting forces on each other. When the secondary island is sufficiently large, this causes it to split into two parts, which then coalesce with the primary island [Figs. 7(d)–7(f)] (the splitting of the secondary island into two is a result of the exact symmetry of our configuration about the x axis: even a slight asymmetry causes the entire secondary island to move either upwards or downwards to coalesce with the primary [25]).

Given small enough η , the secondary current sheets should be unstable to generation of tertiary islands, etc. Also, if the initial flux is not yet exhausted after the secondary island has coalesced with the primary, the primary current sheet can be regenerated via a second collapse (Fig. 1, stage IVb). Given sufficiently large Δ' , the cycle of current-sheet formation—secondary-island generation—coalescence may be repeated several times before saturation is reached.

Stage V: Saturation.—The saturated island width in the limit of small Δ' has recently been calculated by Escande and Ottaviani [26] and by Militello and Porcelli [27], a

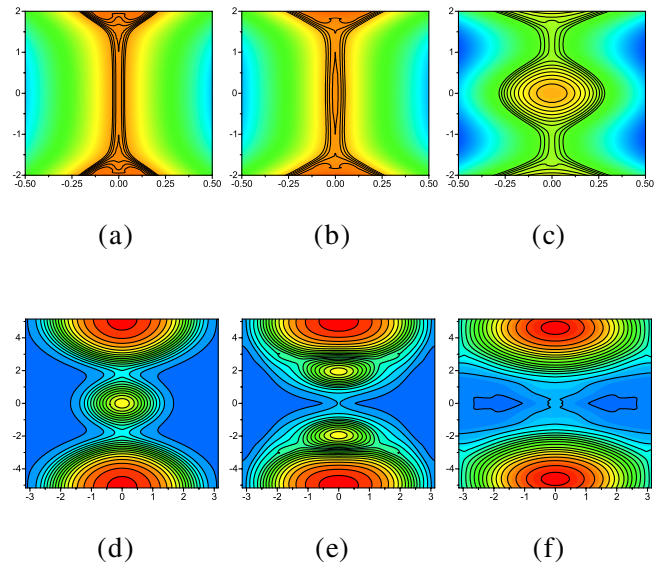


FIG. 7 (color online). Contours of ψ showing the current-sheet instability (a)–(c) and the subsequent nonlinear evolution of the secondary island (d)–(f) for a run with $\Delta' = 40.6$, $\eta = 2.8 \times 10^{-4}$.

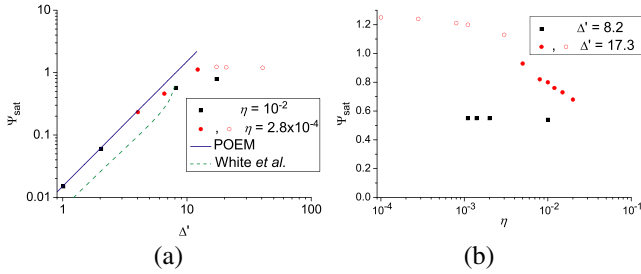


FIG. 8 (color online). (a) Saturated amplitude Ψ_{sat} vs Δ' for different values of η . The theoretical curves by POEM and White *et al.* [28] are also shown. The island width formula (3) has been used to convert W_{sat} calculated by these authors into Ψ_{sat} . (b) Ψ_{sat} vs η for $\Delta' = 8.2, 17.3$. In both plots, open circles are the cases where W_{sat} exceeded the box size.

theory henceforth referred to, using a liberal permutation of the first letters of the authors' surnames, as POEM. They found $W_{\text{sat}} = 2.44a^2\Delta'$, where $a^2 = -\psi_0''(0)/\psi_0'''(0) = 0.125$ for our equilibrium. Figure 8 shows the dependence of the numerically obtained saturated flux on Δ' and η . We plot Ψ_{sat} instead of W_{sat} because, for the largest Δ' values, the island width exceeds the box size L_x (in which case the saturation is likely to be strongly dependent on the equilibrium configuration). For $\Delta' \lesssim 5$, there is excellent agreement with POEM, but not with the earlier theory of White *et al.* [28]. Our study extends the previously published numerical confirmations of POEM for small Δ' [26,27] and traces the Δ' dependence of Ψ_{sat} to and beyond the values of Δ' at which POEM breaks down. The occurrence of the X-point collapse, i.e., whether the saturation is achieved via current-sheet or X-point reconnection, changes the saturated state: Figure 8 shows a jump in Ψ_{sat} at values of Δ' and η for which the X-point collapse took place in stage III. For sufficiently small η , the saturated amplitude does not depend on η [Fig. 8(b)]. Also, Ψ_{sat} appears to reach a plateau for large Δ' [Fig. 8(a)], so that $W_{\text{sat}} \sim$ system size. Note that the collapse can occur only if W_{sat} is larger than Waelbroeck's critical value (Fig. 3), $W_{\text{sat}} > W_c$. Using Eq. (5) and the POEM formula for W_{sat} , this gives $\Delta' \gtrsim 5.2$ in the limit of $\eta \rightarrow 0$.

The new results reported above are the numerical identification of (i) the tearing-mode evolution as a five-stage process, (ii) a criterion for the current-sheet formation [Eq. (5)], (iii) exponential reconnection at the Sweet-Parker rate during the current-sheet stage, (iv) secondary-island generation as a long-wavelength instability of high-aspect-ratio current sheets, followed by formation of secondary current sheets and then by coalescence of the secondary and primary islands, and (v) transition from the saturated state described by the small-island approximation [26,27] to a large- Δ' regime.

A caveat is in order. While stable large- Δ' configurations are often encountered in fusion plasmas, the physics that sets the critical Δ' for instability is still a challenge. This physics, along with a number of kinetic effects known

to be important in various laboratory and astrophysical contexts [29], must, strictly speaking, be a part of any quantitative description of the tearing-mode reconnection in real plasmas.

Discussions with J. Drake, B. Jemella, B. Rogers, M. Shay, and F. Waelbroeck are gratefully acknowledged. This work was supported by Fundação para a Ciência e a Tecnologia, Portuguese Ministry for Science and Higher Education (N. F. L.), the UKAFF (A. A. S.), and the DOE Center for Multiscale Plasma Dynamics.

-
- [1] P. A. Sweet, *Annu. Rev. Astron. Astrophys.* **7**, 149 (1969).
 - [2] J. Dungey, *Phys. Rev. Lett.* **6**, 47 (1961).
 - [3] B. Kadomtsev, *Sov. J. Plasma Phys.* **1**, 389 (1976).
 - [4] H. P. Furth, J. Killeen, and M. N. Rosenbluth, *Phys. Fluids* **6**, 459 (1963).
 - [5] S. C. Cowley, R. M. Kulsrud, and T. S. Hahm, *Phys. Fluids* **29**, 3230 (1986).
 - [6] S. Migliuolo, F. Pegoraro, and F. Porcelli, *Phys. Fluids B* **3**, 1338 (1991).
 - [7] C. Angioni *et al.*, *Plasma Phys. Controlled Fusion* **44**, 205 (2002).
 - [8] P. H. Rutherford, *Phys. Fluids* **16**, 1903 (1973).
 - [9] P. A. Sweet, in *Proceedings of the IAU Symposium 6: Electromagnetic Phenomena in Cosmical Physics* (Cambridge University Press, Cambridge, England, 1958), p. 123.
 - [10] E. N. Parker, *J. Geophys. Res.* **62**, 509 (1957).
 - [11] H. R. Strauss, *Phys. Fluids* **19**, 134 (1976).
 - [12] F. Porcelli *et al.*, *Plasma Phys. Controlled Fusion* **44**, B389 (2002).
 - [13] D. Biskamp, *Nonlinear Magnetohydrodynamics* (Cambridge University Press, Cambridge, 1993).
 - [14] F. L. Waelbroeck, *Phys. Rev. Lett.* **70**, 3259 (1993).
 - [15] B. D. Jemella *et al.*, *Phys. Rev. Lett.* **91**, 125002 (2003).
 - [16] M. Ottaviani and F. Porcelli, *Phys. Plasmas* **2**, 4104 (1995).
 - [17] The exponential growth is not apparent in the γ_{eff} diagnostic of Fig. 1 because in our simulations Ψ grows only by a factor of $\lesssim 10$ during this stage.
 - [18] S. I. Syrovatskii, *Sov. Phys. JETP* **33**, 933 (1971).
 - [19] F. L. Waelbroeck, *Phys. Fluids B* **1**, 2372 (1989).
 - [20] L. Zakharov, B. Rogers, and S. Migliuolo, *Phys. Fluids B* **5**, 2498 (1993).
 - [21] B. D. Jemella, J. F. Drake, and M. A. Shay, *Phys. Plasmas* **11**, 5668 (2004).
 - [22] L. C. Lee and Z. F. Fu, *J. Geophys. Res.* **91**, 6807 (1986).
 - [23] R. S. Steinolfson and G. Van Hoven, *Phys. Fluids* **27**, 1207 (1984).
 - [24] S. V. Bulanov, S. I. Syrovatsky, and J. Sakai, *JETP Lett.* **28**, 177 (1978).
 - [25] This was confirmed by L. Chacon (private communication) using a grid code.
 - [26] D. F. Escande and M. Ottaviani, *Phys. Lett. A* **323**, 278 (2004).
 - [27] F. Militello and F. Porcelli, *Phys. Plasmas* **11**, L13 (2004).
 - [28] R. B. White *et al.*, *Phys. Fluids* **20**, 800 (1977).
 - [29] J. Birn *et al.*, *J. Geophys. Res.* **106**, 3715 (2001).